# On the Energetics of Quadrupedal Bounding With and Without Torso Compliance

Qu Cao and Ioannis Poulakakis

***Abstract*— This paper examines the influence of torso compliance on the efficiency of quadrupedal running with a bounding gait. Two sagittal-plane models, one with and one without torso compliance, are developed in a template setting. The models feature non-trivial leg mass, and are coupled with a simple leg recirculation controller to generate bounding motions. Despite their simplicity, the proposed models are sufficiently expressive to capture the energetics of bounding motions and to assess the contribution of torso flexibility to gait efficiency measured by the cost of transport. Comparisons reveal that torso compliance promotes locomotion performance by reducing energy consumption only at speeds that are sufficiently high.**

## I. Introduction

A series of robotic quadrupeds has been developed following Raibert's pioneering work [1] to explore the prospect of these machines in real-life applications. A variety of dynamic gaits has been implemented on these quadrupeds, including walking [2], trotting [3]–[5] and bounding [6]. An important criterion for assessing the performance of these robots—and their capacity to operate in a power autonomous fashion—is energy efficiency.

One way to improve energy efficiency is to incorporate elastic energy storage elements, i.e., springs, in the robot's mechanical structure. Such compliant elements can be used to recycle energy, thereby reducing the power cost of maintaining the motion. Compliance in quadrupedal robots is generally introduced in the leg structure [5]–[7]. On the other hand, incorporating elastic elements within the robot's torso did not receive much attention. Although quadrupeds with articulated torsos have been recently introduced [8], [9], these robots do not explicitly include compliant elements in their torsos. In contrast, the quadrupedal robot Canid combines torso actuation with leaf springs to capture the effect of torso compliance on motion generation [10].

In parallel with robot design, a variety of models have been proposed to understand the influence of elastic elements within the torso on quadrupedal running. Recognizing the value of reduced-order models, or "templates" [11], in studying the mechanics of legged locomotion, the majority of these efforts focus on conservative spring-mass systems [12]–[16]. In analogy with the Spring Loaded Inverted Pendulum (SLIP) [11], these models feature massless springy legs and focus on periodic gait generation and stability. As a result, they cannot capture the consequences of torso compliance on energy consumption. On the other hand, early results in [17] based on biological observations indicate that torso flexibility could reduce the metabolic cost of transport through recycling part of the kinetic energy required to recirculate the legs. Yet, no models are known to us that are capable of directly measuring the effect of torso compliance on gait efficiency. This is not to say that models with segmented torsos have not been proposed to assess the cost of transport of quadrupedal running gaits; in fact, [18]–[20] provide relevant computations. However, in all these models, the torso is actuated and does not include any compliant elements.

To probe the relationship between elastic elements within the torso structure and energy consumption in the context of quadrupedal running, this paper compares two sagittal-plane bounding models in a template setting, one with a segmented *flexible*, unactuated torso and one with a *rigid* undeformable torso. Both models include legs with non-trivial mass, intended to capture the energy cost associated with leg recirculation. Since our objective is to characterize the energy cost associated with the generation of a nominal gait cycle, a simple controller is employed that merely places the legs during flight in anticipation of touchdown; no control is exerted at the hip when a leg is on the ground. The resulting motions are periodic, but not necessarily stable. By comparing the cost of transport of bounding using the two models in a non-dimensional setting, it is deduced that torso compliance significantly enhances energy efficiency, but *only* when the Froude number exceeds a particular value. Interestingly, this value corresponds to the Froude number at which transitions from trotting to galloping are observed in animals with drastically different morphological characteristics [21]. These results suggest that in order to take advantage of torso compliance in improving the efficiency of quadrupedal robots, these robots must be capable of realizing highly dynamic motions. Otherwise, the positive effect of torso compliance on energy efficiency may be lost.

The structure of the paper is as follows. Section II introduces the two models and derives their dynamic equations in a non-dimensional form. Section III describes the process used to numerically generate energy-efficient bounding motions via optimization. Section IV discusses the energetics of the two models and highlights the effects of torso compliance. Section V concludes the paper.

## II. Non-dimensional Reduced-order Models

To study the effect of torso compliance on the energetics of bounding in a template setting, two sagittal-plane quadrupedal models—one with a rigid torso and one with a flexible segmented torso—are considered; see Fig. 1. The

Q. Cao and I. Poulakakis are with the Department of Mechanical Engineering, University of Delaware, Newark, DE 19716, USA; e-mail: {caoqu, poulakas}@udel.edu. This work is supported in part by NSF grant CMMI-1130372 and ARL contract W911NF-12-1-0117.

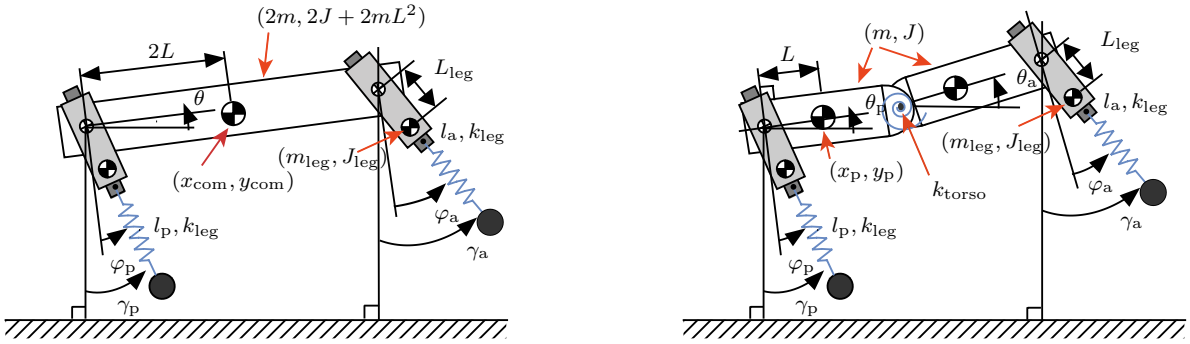


Fig. 1. Two sagittal-plane quadrupedal models used to study the energetics of bounding motion. (a) Rigid torso model; (b) Flexible torso model.

legs in each model are identical; each consists of an upper segment with mass $m_{\rm leg}$ and moment of inertia $J_{\rm leg}$ about its center of mass (COM) and a lower segment represented by a massless prismatic spring of stiffness $k_{\rm leg}$. The natural length of the leg, i.e., the distance between the hip and the toe when the leg spring is uncompressed, is denoted by $l_0$ and the distance between the COM of the leg and the hip joint is $L_{\rm leg}$. The toe-ground interaction is modeled as an unactuated, frictionless pin joint.

In the flexible torso model, it is assumed that the anterior and posterior parts of the torso are identical with mass $m$, moment of inertia $J$ about their COM and hip-to-COM spacing $L$; see Fig. 1(b). A rotational spring is inserted between the two segments to introduce flexibility that produces a torque given by $k_{\rm torso}(\theta_{\rm a} - \theta_{\rm p} - \theta_{\rm rest})$, where $k_{\rm torso}$ is the stiffness of the spring, $\theta_{\rm a}$, $\theta_{\rm p}$ are the pitch angles of the two segments and $\theta_{\rm rest}$ represents the rest angle of the spring. For fair comparison, the torso mass, hip-to-COM distance and moment of inertia of the torso about the COM in the rigid-torso model are $2m$, $2L$ and $2J + 2mL^2$, respectively.

The bounding gait, which can be considered as a limiting case of galloping, is depicted in Fig. 2. Depending on the state of the legs and the configuration of the torso of the flexible-torso model, bounding can be divided into four phases: the posterior stance phase, denoted by "sp", when only the posterior (back) leg is on the ground; the anterior stance phase, denoted by "sa", in which only the anterior (front) leg is in contact with the ground; the extended flight phase, denoted by "fe", when both legs are in the air and the torso exhibits a convex configuration and the gathered flight phase, denoted by "fg", when both legs are in the air and the torso is concave. The rigid torso bounding follows the sequence of Fig. 2, albeit there is no distinction in the torso configuration during the extended and gathered flight.

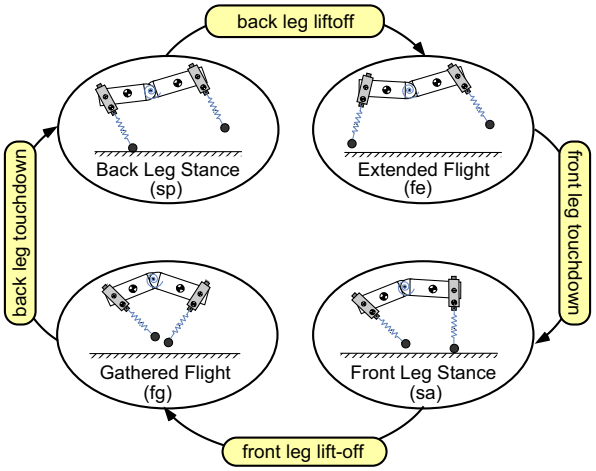


Fig. 2. Bounding phases and events.

### A. Continuous-time dynamics in non-dimensional form

For $i \in \{\rm sp, sa, fg, fe\}$, the equations of motion for both models can be derived using the method of Lagrange, and can be brought in state-space form as

$$\dot{x}_i = f_i(x_i) + g_i(x_i)u_i \tag{1}$$

where $u_i := (u_{i,\rm p}, u_{i,\rm a})'$ represents the inputs at the posterior and anterior hip joints and $x_i := (q_i, \dot{q}_i)'$ are the corresponding states, with the configuration variables $q_i$ defined as

$$q_i := \begin{cases} (l_{\rm p}, \varphi_{\rm p}, \varphi_{\rm a}, \theta_{\rm p}, \theta_{\rm a})' & \text{for } \ i = \rm sp, \\ (l_{\rm a}, \varphi_{\rm p}, \varphi_{\rm a}, \theta_{\rm p}, \theta_{\rm a})' & \text{for } \ i = \rm sa, \\ (x_{\rm p}, y_{\rm p}, \varphi_{\rm p}, \varphi_{\rm a}, \theta_{\rm p}, \theta_{\rm a})' & \text{for } \ i \in \{\rm fg, fe\} \end{cases} \tag{2}$$

for the flexible-torso model and

$$q_i := \begin{cases} (l_{\rm p}, \varphi_{\rm p}, \varphi_{\rm a}, \theta)' & \text{for } \ i = \rm sp, \\ (l_{\rm a}, \varphi_{\rm p}, \varphi_{\rm a}, \theta)' & \text{for } \ i = \rm sa, \\ (x_{\rm com}, y_{\rm com}, \varphi_{\rm p}, \varphi_{\rm a}, \theta)' & \text{for } \ i \in \{\rm fg, fe\} \end{cases} \tag{3}$$

for the rigid-torso model.

The physical properties of the two models can be captured by the following parameters

$$\{m, m_{\rm leg}, J, J_{\rm leg}, l_0, L_{\rm leg}, L, k_{\rm torso}, k_{\rm leg}\}. \tag{4}$$

To provide a platform-independent analysis, the dynamics of the system can be transformed in a non-dimensional form. By selecting the characteristic time scale $\tau$ as $\tau := \sqrt{l_0/g}$, where $g$ is the gravitational acceleration, the configuration variables in (2) and (3) and their derivatives obtain the form:

$$\zeta^* := \zeta/l_0, \quad \dot{\zeta}^* := \tau\dot{\zeta}/l_0, \quad \ddot{\zeta}^* := \tau^2\ddot{\zeta}/l_0, \tag{5}$$

for $\zeta \in \{x_{\rm p}, y_{\rm p}, x_{\rm com}, y_{\rm com}, l_{\rm p}, l_{\rm a}\}$ and

$$\psi^* := \psi, \quad \dot{\psi}^* := \tau\dot{\psi}, \quad \ddot{\psi}^* := \tau^2\ddot{\psi}, \tag{6}$$

for $\psi \in \{\varphi_{\rm p}, \varphi_{\rm a}, \theta_{\rm p}, \theta_{\rm a}, \theta\}$ where the superscript " * " denotes a dimensionless quantity. Finally, the non-dimensional input torque $u_i^*$ is defined as:

$$u_i^* := u_i/(mgl_0) \tag{7}$$

Substitution of (5) and (6) into (1) reduces the parameters in (4) to the following seven dimensionless quantities:

$$\{I, M_{\rm leg}, I_{\rm leg}, d, d_{\rm leg}, \kappa_{\rm torso}, \kappa_{\rm leg}\} \tag{8}$$

defined in Table I. One more non-dimensional quantity defined in Table I is the Froude number, $Fr$, used to describe the average forward running speed $\bar{v}$.

TABLE I
NON-DIMENSIONAL PARAMETERS

| | |
|---|---|
| Relative torso moment of inertia | $I := J/(mL^2)$ |
| Relative leg mass | $M_{\rm leg} := m_{\rm leg}/m$ |
| Relative leg moment of inertia | $I_{\rm leg} := J_{\rm leg}/(m_{\rm leg} l_0^2)$ |
| Relative hip-to-torso COM distance | $d := L/l_0$ |
| Relative hip-to-leg COM distance | $d_{\rm leg} := L_{\rm leg}/l_0$ |
| Relative torso stiffness | $\kappa_{\rm torso} := k_{\rm torso}/(mgl_0)$ |
| Relative leg stiffness | $\kappa_{\rm leg} := k_{\rm leg} l_0/(mg)$ |
| Froude number | $Fr := \bar{v}/\sqrt{gl_0}$ |

### B. Event-based transitions

The continuous-time phases are separated by touchdown and liftoff events as in Fig. 2.

*1) Flight-to-stance transitions:* The flight phase terminates when the vertical distance between the toe of either the posterior or the anterior leg and the ground becomes zero. Due to the non-zero mass of the upper part of each leg, an impact occurs at touchdown, which is modeled according to [22, Section 3.4].

*2) Stance-to-flight transitions:* In general, transitions from stance to flight happen when the ground reaction force becomes zero. Because of the assumption of massless springy lower legs, liftoff is assumed to occur when the leg spring extends to its natural length.

## III. GENERATION OF PERIODIC MOTIONS

Our purpose in this work is to characterize the impact of torso flexibility on energy consumption. As a result, the objective of the controller used to generate bounding is to recirculate the leg during the flight phase and to replace the energy lost at impacts. No control is exerted for the leg that is in contact with the ground; the corresponding hip joint is passive, similarly to the conservative massless models in [23]. Note that the resulting motions are not necessarily stable and further control action is required to guarantee stability. Finally, to avoid cumbersome notation, hereafter we neglect " * " with the understanding that all the variables are the non-dimensional ones defined in (5), (6) and (7).

### A. Leg recirculation control

As was mentioned above, we focus on the hip joint of the leg that is in flight. In our study, the corresponding hip joint torque $u_i$ in (1) will be determined by imposing suitably designed output functions in the form of (virtual) holonomic constraints. It is mentioned that other control methods such as the PID controller in [19] can also be used. In what follows, we derive the controller for the flexible-torso model; the corresponding controller for the rigid-torso model can be derived in an analogous fashion, and is omitted for brevity.

To the dynamics (1) we associate the output function

$$y_i = h_i(q_i, \alpha_i) := q_{{\rm c},i} - h_i^{\rm d}(s_i(q_i), \alpha_i) \tag{9}$$

where $q_{{\rm c},i}$ is the controlled variable, which in our case is selected to be the posterior (anterior) absolute leg angle in the anterior (posterior) stance phase and in the extended (gathered) flight phase, i.e.,

$$q_{{\rm c},i} := \begin{cases} \gamma_{\rm p} = \varphi_{\rm p} + \theta_{\rm p} & \text{for } \ i \in \{\rm sa, fe\}, \\ \gamma_{\rm a} = \varphi_{\rm a} + \theta_{\rm a} & \text{for } \ i \in \{\rm sp, fg\}. \end{cases} \tag{10}$$

In all the phases, the desired evolution $h_i^{\rm d}$ is described via 5-th order Beziér polynomials with coefficients $\alpha_i := \{\alpha_{i,k}\}_{k=0,\ldots,5}$, i.e.,

$$h_i^{\rm d}(s_i(q_i), \alpha_i) = \sum_{k=0}^{5} b_{i,k}(s_i(q_i))\alpha_{i,k}, \tag{11}$$

where the terms $b_{i,k}$ are given by

$$b_{i,k}(s_i) := \frac{5!}{k!(5-k)!} s_i^k (1-s_i)^{5-k}, \tag{12}$$

in which the dependence on $q_i$ has been suppressed, and $s_i$ is the strictly monotonic quantity

$$s_i := \frac{\gamma^{\max} - \gamma}{\gamma^{\max} - \gamma^{\min}}. \tag{13}$$

In (13)

$$\gamma := \begin{cases} \gamma_{\rm p} & \text{for } \ i \in \{\rm sp, fg\}, \\ \gamma_{\rm a} & \text{for } \ i \in \{\rm sa, fe\}, \end{cases} \tag{14}$$

and $\gamma^{\max}$ and $\gamma^{\min}$ are the maximum and minimum values of $\gamma$ in the corresponding phase. Note that with these definitions, the output functions (9) are solely dependent on the configuration variables $q_i$ and the parameters $\alpha_i$ associated with the polynomials (11), and can therefore be interpreted as (virtual) holonomic constraints.

As a final note, the monotonicity of $s_i$ in (13) is important, since it allows us to replace time, effectively coordinating the motions of the legs with respect to an "internal" clock, as in [22]. More details on establishing the monotonicity of $s_i$, for $i \in \{\rm sa, sp, fg, fe\}$ can be found in the Appendix.

To impose the constraints (9) on the dynamics (1) we differentiate (9) twice with respect to time to obtain

$$\frac{d^2 y_i}{d\tau^2} = L_{f_i}^2 h_i(x_i, \alpha_i) + L_{g_i} L_{f_i} h_i(q_i, \alpha_i) u_i, \tag{15}$$

where, in accordance with the notation in [22], $L_{f_i}^2 h_i$ and $L_{g_i} L_{f_i} h_i$ are the Lie derivatives of the output function $h_i$ defined by (9) along the vector fields $f_i$ and $g_i$ that participate in (1). Since one of the hip torques in $u_i$ is either $0$ or determined by the swing-leg retraction (SR) controller (22) explained in the Appendix, the other hip torque will be

TABLE II

CONTROL ACTION IN EACH PHASE

| | $i$ = sa | $i$ = fg | $i$ = sp | $i$ = fe |
|---|---|---|---|---|
| $u_{i,\mathrm{a}}$ | 0 | zeroing (15) | zeroing (15) | SR |
| $u_{i,\mathrm{p}}$ | zeroing (15) | SR | 0 | zeroing (15) |

computed to ensure $d^2y_i/d\tau^2 = 0$; Table II summarizes the control action in each phase. With these inputs, the dynamics (1) in each phase can be written in closed-loop form as

$$\dot{x}_i = f_i^{\mathrm{cl}}(x_i, \alpha_i). \tag{16}$$

where $\alpha_i$ includes all the parameters associated with the construction of the output functions for each phase.

### B. Poincaré return map

To determine the existence of periodic bounding motions, we numerically integrate the closed-loop dynamics for each phase according to the phase sequence of Fig. 2 starting with the anterior leg liftoff to construct the return map $\mathcal{P}$ as

$$z[k+1] = \mathcal{P}(z[k], \alpha[k]), \tag{17}$$

where $\alpha$ includes all the parameters $\alpha_i$ introduced by the continuous-time controllers designed in Section III-A, and $z := (\varphi_{\mathrm{p}}, \varphi_{\mathrm{a}}, \theta_{\mathrm{p}}, \theta_{\mathrm{a}}, l_{\mathrm{a}}, \dot{\varphi}_{\mathrm{p}}, \dot{\varphi}_{\mathrm{a}}, \dot{\theta}_{\mathrm{p}}, \dot{\theta}_{\mathrm{a}})$ for the flexible-torso model and $z := (\varphi_{\mathrm{p}}, \varphi_{\mathrm{a}}, \theta, l_{\mathrm{a}}, \dot{\varphi}_{\mathrm{p}}, \dot{\varphi}_{\mathrm{a}}, \dot{\theta})$ for the rigid-torso model. Then, the problem of computing periodic bounding gaits is reduced to the problem of finding a state vector $z$ and parameters $\alpha$ so that

$$z - \mathcal{P}(z, \alpha) = 0. \tag{18}$$

### C. Optimization

To compare energy consumption for the two models, we use the cost of transport (COT) [24], which is defined as the total energy consumed divided by the distance travelled and the weight of the model, i.e.

$$c = \frac{1}{2(1+M_{\mathrm{leg}})TFr} \int_0^T (|u_{\mathrm{a}}\dot{\varphi}_{\mathrm{a}}| + |u_{\mathrm{p}}\dot{\varphi}_{\mathrm{p}}|)d\tau, \tag{19}$$

where all the quantities are non-dimensional and $T$ is the stride period. Note that the definition of the COT by (19) corresponds to the mechanical cost of transport; the actuator efficiency is not considered. With this criteria for measuring energy efficiency, the search for efficient bounding motions can be cast as a constrained optimization problem

$$\min\{c(z,\alpha)\} \quad \text{such that} \quad z = \mathcal{P}(z,\alpha), \tag{20}$$

which is solved numerically using MATLAB's `fmincon`.

## IV. RESULTS

Using the optimization framework described in Section III, the COT of bounding gaits that are realized in both the rigid and flexible torso models can be compared for different speeds and geometries. We begin our discussion with Fig. 3, which shows the COT computed for different relative hip-to-COM distances $d \in \{0.34, 0.38, 0.42\}$ and for various traveling velocities, as these are captured by the Froude number $Fr \in [1.5, 5.0]$. The rest of the parameters are kept constant and are given in Table III. It should be mentioned here that all the bounding motions corresponding to the flexible-torso model exhibit pronounced torso oscillations, and that below a minimum speed no cyclic motions can be generated for this model.

TABLE III

NON-DIMENSIONAL MECHANICAL PARAMETERS OF THE MODELS

| **Parameters** | $I$ | $M_{\mathrm{leg}}$ | $I_{\mathrm{leg}}$ | $L_{\mathrm{leg}}$ | $\kappa_{\mathrm{leg}}$ | $\kappa_{\mathrm{tor}}$ | $\theta_{\mathrm{rest}}$ |
|---|---|---|---|---|---|---|---|
| **Values** | 1.8 | 0.1 | 0.01 | 0.25 | 25.8 | 5.5 | -0.17 |

It is clear from Fig. 3 that the energy consumption increases with the traveling speed in both models. However, compared to the flexible-torso model, the energy cost in the rigid-torso model increases at a faster rate as the Froude number grows. This is evident from Fig. 3, where it is seen that the difference between the COT for the flexible- and rigid-torso models is amplified at higher Froude numbers. At low Froude numbers, it was either impossible to compute fixed points in the flexible-torso model, as in Fig. 3(a) and 3(b), or the fixed points resulted in relatively higher COT than those of the rigid-torso model, as in Figs. 3(c). These observations imply that the benefits of torso flexibility in terms of energy efficiency are most appreciated at higher traveling speeds. Finally, Fig. 3(c) shows that the threshold value for the Froude number beyond which the flexible-torso model becomes more efficient is approximately equal to $1.8$[1]. It is interesting to note that this value corresponds to the transition from trotting to galloping, which is the same in animals with drastically different geometries[2] [21], such as horses and dogs [25], [26].

The improved efficiency of the flexible-torso model at higher traveling speeds can be attributed to the contribution of the torso's dorsoventral oscillations to recirculating the legs. According to this hypothesis—which was put forward in [27]—as the torso flexes it facilitates the motion of the anterior leg backward and of the posterior leg forward, and vice versa for the case where the torso extends. The model of Fig. 1(b) is well suited for analyzing the effect of leg recirculation on efficiency; for, it effectively measures the energetic cost associated with the repositioning of the swing leg in anticipation of touchdown. In more detail, Fig. 4 depicts the evolution of the absolute and relative leg angles for one of the fixed points of Fig. 3(c); namely, the fixed point corresponding to[3] $d = 0.42$ and $Fr = 3.0$. Figure 4 shows that, for the rigid-torso model, the evolution of the absolute angle of the posterior, $\gamma_{\mathrm{p}}$, and anterior, $\gamma_{\mathrm{a}}$, legs does not differ significantly from that of the corresponding relative angles $\varphi_{\mathrm{p}}$ and $\varphi_{\mathrm{a}}$. By way of contrast, the differences between $\gamma_{\mathrm{p}}$ and $\varphi_{\mathrm{p}}$, and $\gamma_{\mathrm{a}}$ and $\varphi_{\mathrm{a}}$ are much larger in the flexible-torso model. For example, the absolute angle of the anterior leg $\gamma_{\mathrm{a}}$ evolves in $[-0.77, 0.49]$ while the range of the anterior leg angle relative

[1]This value is also observed in fixed points computed for $d > 0.42$ which are not shown here.

[2]In biological studies, the Froude number is defined as $Fr := \bar{v}^2/(gl_0)$, which is the square of our definition in Table I.

[3]Similar behavior as in Fig. 4 is exhibited by the rest of the fixed points.

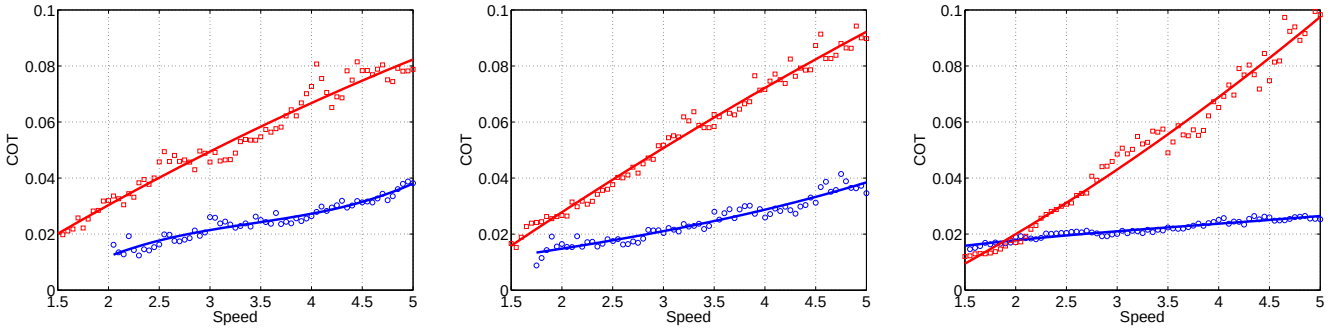


(a) $d = 0.34$ (b) $d = 0.38$ (c) $d = 0.42$

Fig. 3. COT of flexible-torso (blue circles) and rigid-torso (red squares) models of different speeds and relative hip-to-COM distance. The continuous lines are fitted 3rd-order polynomials.

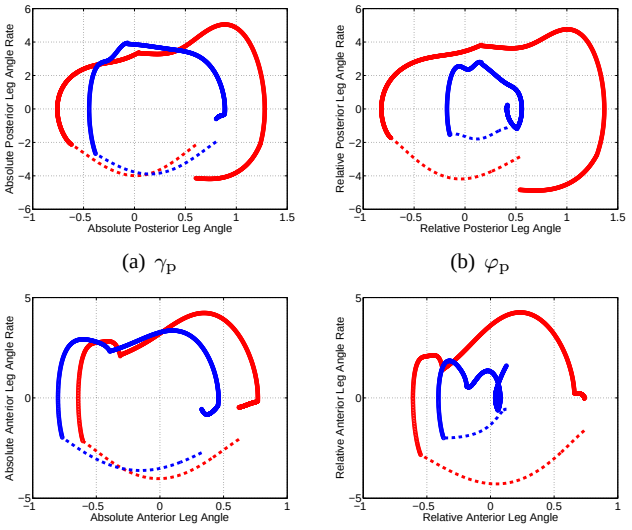


(a) $\gamma_{\mathrm{p}}$ (b) $\varphi_{\mathrm{p}}$

(c) $\gamma_{\mathrm{a}}$ (d) $\varphi_{\mathrm{a}}$

Fig. 4. The phase portrait of the posterior (a, b) and anterior (c, d) leg angles for a bounding gait at $Fr = 3.0$ with $d = 0.42$ for rigid-torso (red) and flexible torso (blue). The dotted lines represent the stance phases. The discontinuity in leg angle rate is due to the impacts at touchdown.

to the torso $\varphi_{\mathrm{a}}$ is $[-0.40, 0.13]$. Unlike the pitch motion of the rigid-torso model, which shows little effect on leg recirculation, the torso's flexion/extension oscillations in the flexible-torso model significantly contributes to repositioning the leg during flight.

As a final comment, it can be seen from Figs. 5(a), 5(c) and 5(e) that as the forward speed increases, the stride frequency of the flexible-torso model remains almost constant. Correspondingly, Figs. 5(b), 5(d) and 5(f) demonstrate a linear relationship between the forward speed and the stride length for the flexible-torso model. This observation is consistent with biological data showing that at high-speed running gaits mammals increase their velocity by increasing stride length instead of stride frequency [26].

## V. Conclusions

This paper studies the energetics of quadrupedal running with a bounding gait in the context of two reductive sagittal-plane models with and without torso compliance. Contrary to other template-like models of bounding that have appeared in the literature, the proposed models feature non-trivial leg mass and their dynamic equations are derived in a non-dimensional form. The models are coupled with a simple controller that is capable of generating cyclic bounding motions without, though, ensuring their stability. The controller merely recirculates the legs in flight; no control action is exerted on the legs in contact with the ground. Based on the analysis of the corresponding return map, a number of bounding gaits that minimize the COT at different traveling speeds and torso geometries have been computed. Comparisons among these different gaits based on

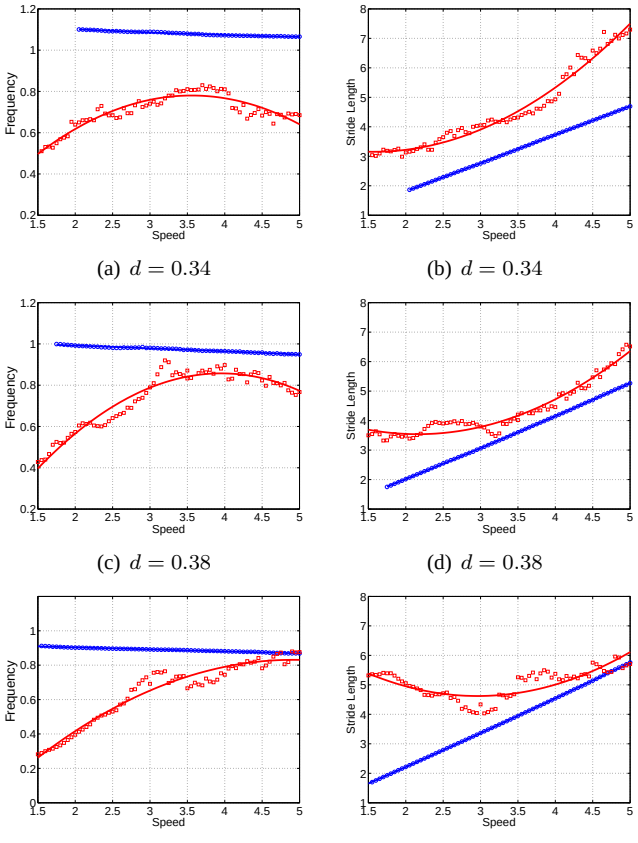


(a) $d = 0.34$ (b) $d = 0.34$

(c) $d = 0.38$ (d) $d = 0.38$

(e) $d = 0.42$ (f) $d = 0.42$

Fig. 5. Stride frequency (a, c, e) and stride length (b, d, f) of flexible-torso (blue circles) and rigid-torso (red squares) models of various speeds and hip-to-COM distances. The continuous lines are fitted 3rd-order polynomials.

the corresponding COT for the two models reveal a number of interesting observations. For example, torso flexibility enhances gait efficiency only when the running speed is beyond a threshold value, which interestingly matches the transition from trotting to galloping speed in animals of different geometries and structures. These results are relevant to the design and control of quadrupedal robots that harness compliant structures in their torsos and legs to realize highly dynamic and efficient running motions.

## APPENDIX

The monotonicity of $s_i$ in the stance phases $i \in \{\mathrm{sa}, \mathrm{sp}\}$ is an immediate consequence of the evolution of the absolute leg angles $\gamma_\mathrm{p}$ and $\gamma_\mathrm{a}$; for, the stance leg is continuously swept backward. During the flight phases, the monotonicity of $s_i$ can be guaranteed through proper choice of the coefficients of the Beziér polynomials, in conjunction with a swing-leg retraction controller, like the one proposed in [28]. This controller minimizes the horizontal speed of the toe relative to the ground at touchdown, thereby reducing the energy lost due to the impact. To provide more details, consider $s_i$ in the gathered flight; i.e., $s_\mathrm{fg}$. Prior to entering the gathered flight—that is, at the end of the anterior stance—known properties of the Beziér polynomials [22, Section 6.2] can be used to write the swing velocity of the posterior leg as

$$\dot{\gamma}_\mathrm{p} = 5(\alpha_{\mathrm{sa},5} - \alpha_{\mathrm{sa},4})\dot{s}_\mathrm{sa}. \tag{21}$$

Since $s_\mathrm{sa}$ is strictly monotonically increasing in stance-anterior, choosing $\alpha_{\mathrm{sa},5} < \alpha_{\mathrm{sa},4}$ will force the posterior leg to swing backward; that is, $\dot{\gamma}_\mathrm{p} < 0$ as we enter the ensuing gathered flight phase. Choosing the input torque $u_\mathrm{p}$ during the gathered flight according to the prescription

$$u_\mathrm{p} = K_\mathrm{p}\dot{x}_\mathrm{p}^\mathrm{toe} \tag{22}$$

where $K_\mathrm{p} < 0$ and $\dot{x}_\mathrm{p}^\mathrm{toe}$ is the forward velocity of the posterior toe relative to the ground allows us to choose the constants $\alpha_{\mathrm{sa},5}, \alpha_{\mathrm{sa},4}$ in (21) and $K_\mathrm{p}$ in (22) to make $\gamma_\mathrm{p}$ monotonically decreasing during the gathered flight. The same procedure is used to ensure the monotonicity of $s_\mathrm{fe}$ in the extended flight phase, resulting in introducing a constant $K_\mathrm{a}$. Note that $K_\mathrm{p}$ and $K_\mathrm{a}$ are incorporated in the parameters $\alpha$ used in the optimization problem of Section III-C.

## REFERENCES


[1] M. H. Raibert, *Legged Robots that Balance*. Cambridge, MA: MIT Press, 1986.

[2] Y. Fukuoka, H. Kimura, and A. H. Cohen, "Adaptive dynamic walking of a quadruped robot on irregular terrain based on biological concepts," *The International Journal of Robotics Research*, vol. 23, no. 10-11, pp. 1059–1073, 2004.

[3] M. Raibert, K. Blankespoor, G. Nelson, R. Playter, and the BigDog Team, "BigDog, the rough-terrain quadruped robot," in *Proceedings of the 17th IFAC World Congress*, Seoul, Korea, July 2008, pp. 10 822–10 825.

[4] C. Semini, N. G. Tsagarakis, E. Guglielmino, M. Focchi, F. Cannella, and D. G. Caldwell, "Design of HyQ - a hydraulically and electrically actuated quadruped robot," *Proceedings of the IMechE Part I: Journal Systems and Control Engineering*, vol. 225, no. 6, pp. 831–849, 2011.

[5] M. Bloesch, S. Coros, M. A. Hoepflinger, R. Siegwart, C. Gehring, and M. Hutter, "Control of dynamic gaits for a quadrupedal robot," in *Proceedings of the IEEE International Conference on Robotics and Automation*, 2013.

[6] I. Poulakakis, J. Smith, and M. Buehler, "Modeling and experiments of untethered quadrupedal running with a bounding gait: The Scout II robots," *The International Journal of Robotics Research*, vol. 24, no. 4, pp. 239–256, 2005.

[7] G. A. Folkertsma, S. Kim, and S. Stramigioli, "Parallel stiffness in a bounding quadruped with flexible spine," in *Proceedings of the IEEE/RSJ International Conference on Intelligent Robots and Systems*, 2012, pp. 2210–2215.

[8] S. Seok, A. Wang, M. Y. Chuah, D. Otten, J. Lang, and S. Kim, "Design principles for highly efficient quadrupeds and implementation on the MIT cheetah robots," in *Proceedings of the IEEE International Conference on Robotics and Automation*. IEEE, 2013, pp. 3307–3312.

[9] M. Khoramshahi, A. Sprowitz, A. Tuleu, M. Ahmadabadi, and A. Ijspeert, "Benefits of an active spine supported bounding locomotion with a small compliant quadruped robot," in *Proceedings of the IEEE International Conference on Robotics and Automation*, 2013, pp. 3329–3334.

[10] J. L. Pusey, J. M. Duperret, G. C. Haynes, R. Knopf, and D. E. Koditschek, "Free-standing leaping experiments with a power-autonomous elastic-spined quadruped," in *SPIE Defense, Security, and Sensing*, 2013, pp. 87 410W–87 410W.

[11] R. Full and D. E. Koditschek, "Templates and anchors: Neuromechanical hypotheses of legged locomotion on land," *Journal of Experimental Biology*, vol. 202, pp. 3325–3332, 1999.

[12] P. Nanua, "Dynamics of a galloping quadruped," Ph.D. dissertation, Ohio State University, 1992.

[13] J. E. Seipel, "Analytic-holistic two-segment model of quadruped back-bending in the sagittal plane," in *ASME Mechanisms and Robotics Conference*, vol. 6, 2011, pp. 855–861.

[14] Q. Deng, S. Wang, W. Xu, J. Mo, and Q. Liang, "Quasi passive bounding of a quadruped model with articulated spine," *Mechanism and Machine Theory*, vol. 52, pp. 232–242, 2012.

[15] Q. Cao and I. Poulakakis, "Quadrupedal bounding with a segmented flexible torso: passive stability and feedback control," *Bioinspiration & Biomimetics*, vol. 8, no. 4, p. 046007, 2013.

[16] R. Yamasaki, Y. Ambe, S. Aoi, and F. Matsuno, "Quadrupedal bounding with spring-damper body joint," in *Proceedings of the IEEE/RSJ International Conference on Intelligent Robots and Systems*, 2013, pp. 2345–2350.

[17] R. Alexander, N. J. Dimery, and R. F. Ker, "Elastic structures in the back and their role in galloping in some mammals," *Journal of Zoology A*, vol. 207, pp. 467–482, 1985.

[18] R. M. Alexander, "Why mammals gallop," *American Zoologist*, vol. 28, no. 1, pp. 237–245, 1988.

[19] U. Culha and U. Saranli, "Quadrupedal bounding with an actuated spinal joint," in *Proceedings of the IEEE International Conference on Robotics and Automation*, 2011, pp. 1392–1397.

[20] B. M. Haueisen, "Investigation of an articulated spine in a quadruped robotic system," Ph.D. dissertation, The University of Michigan, 2011.

[21] R. Alexander, "Optimization and gaits in the locomotion of vertebrates," *Physiological Reviews*, vol. 69, no. 4, pp. 1199–1227, 1989.

[22] E. R. Westervelt, J. W. Grizzle, C. Chevallereau, J. H. Choi, and B. Morris, *Feedback Control of Dynamic Bipedal Robot Locomotion*. Taylor & Francis/CRC Press, 2007.

[23] Q. Cao and I. Poulakakis, "Passive quadrupedal bounding with a segmented flexible torso," in *Proceedings of the IEEE/RSJ International Conference on Intelligent Robots and Systems*, 2012, pp. 2484–2489.

[24] S. H. Collins, A. Ruina, R. Tedrake, and M. Wisse, "Efficient bipedal robots based on passive-dynamic walkers," *Science*, vol. 307, pp. 1082–85, 2005.

[25] D. F. Hoyt and C. R. Taylor, "Gait and the energetics of locomotion in horses." *Nature*, vol. 292, pp. 239 – 240, 1981.

[26] L. D. Maes, M. Herbin, R. Hackert, V. L. Bels, and A. Abourachid, "Steady locomotion in dogs: temporal and associated spatial coordination patterns and the effect of speed," *Journal of Experimental Biology*, vol. 211, no. 1, pp. 138–149, 2008.

[27] R. M. Alexander, "Three uses for springs in legged locomotion," *The International Journal of Robotics Research*, vol. 9, no. 2, pp. 53–61, 1990.

[28] A. Seyfarth, H. Geyer, and H. Herr, "Swing leg retraction: A simple control model for stable running," *Journal of Experimental Biology*, vol. 206, pp. 2547–2555, 2003.